Palaeobiological inferences based on long bone epiphyseal and diaphyseal structure - the forelimb of xenarthrans (Mammalia)

Amson, E.[1,2] and Nyakatura, J.A.[2]

[1]Museum für Naturkunde, Leibniz-Institut für Evolutions- und Biodiversitätsforschung, Berlin, Germany

[2]AG Morphologie und Formengeschichte, Institut für Biologie & *Bild Wissen Gestaltung. Ein interdisziplinäres Labor*, Humboldt-Universität, Berlin, Germany

Abstract

Trabecular architecture (i.e., the main orientation of the bone trabeculae, their relative number, mean thickness, spacing, etc.) has been shown experimentally to adapt with extreme accuracy and sensitivity to the loadings applied to the bone during life. However, the potential of trabecular parameters used as a proxy for the mechanical environment of an organism's organ to help reconstruct the lifestyle of extinct taxa has only recently started to be exploited. Furthermore, these parameters are rarely combined to the long-used mid-diaphyseal parameters to inform such reconstructions. Here we investigate xenarthrans, for which functional and ecological reconstructions of extinct forms are particularly important in order to inform our macroevolutionary understanding of their main constitutive clades, i.e., the Tardigrada (sloths), Vermilingua (anteaters), and Cingulata (armadillos and extinct close relatives). The lifestyles of modern xenarthrans can be classified as fully terrestrial and highly fossorial (armadillos), arboreal (partly to fully) and hook-and-pull digging (anteaters), or suspensory (fully arboreal) and non-fossorial (sloths). The degree of arboreality and fossoriality of some extinct forms, "ground sloths" in particular, is highly debated. We used

high-resolution computed tomography to compare the epiphyseal 3D architecture and mid-diaphyseal structure of the forelimb bones of extant and extinct xenarthrans. The comparative approach employed aims at inferring the most probable lifestyle of extinct taxa, using a phylogenetically informed discriminant analysis. Several challenges were identified, and no extinct sloths were here ascribed to one of the extant xenarthran lifestyles. Differing from that of the larger "ground sloths", the bone structure of the small-sized *Hapalops* (Miocene of Argentina), however, was found as significantly more similar to that of extant sloths, even when accounting for the phylogenetic signal.

Keywords: Bone structure; Forelimb; Locomotion; Palaeobiological inferences; Trabeculae; Xenarthra

Introduction

Bone structure is intensively studied in analyses concerned with functional anatomy because it is argued to be extremely plastic. While a genetic blueprint influences bone structure, it has been shown to adapt during life (and especially at an early ontogenetic stage) to its mechanical environment (Ruff et al. 2006). This was argued for trabecular bone, which reacts to loading with great accuracy and sensitivity (Barak et al. 2011). This was also argued for cortical bone, even though the latter is excepted to be less plastic, at least in part due to its lower remodeling rate (see review of Kivell, 2016). Comparative studies focusing on either trabeculae or cortical structure leveraged this great plasticity to associate structural phenotypes to lifestyles or functional uses of a limb. Because fossil bone cross-sections at mid-diaphysis were produced for over a century and a half (Kolb et al. 2015), a large number of mid-diaphyseal data related to extinct taxa was acquired, and successfully exploited for palaeobiological inferences (e.g., Germain & Laurin, 2005). Fossil three-dimensional (3D) trabecular architecture was much less investigated, as, to our knowledge, only few studies were published, which are all focussing on primates (DeSilva & Devlin 2012; Barak et al. 2013; Su et al. 2013; Skinner et al. 2015; Su & Carlson 2017; Ryan et al. 2018).

Because both trabecular and cortical structure have yielded a functional signal, combining them in a single analysis could potentially help in our endeavours to associate a bone overall structure to a loading regime, and, eventually, a function. This combined analysis has previously been achieved, on extant taxa, via different approaches. Based on epiphyseal regions of interest (ROIs) and mid-diaphyseal sections, Shaw & Ryan (2012) examined both compartments in the humerus and femur of anthropoids (see also Lazenby et al. (2008) for handedness within humans). They measured individual trabecular and mid-diaphyseal parameters, but did not combine the latter in a single test. Another approach, termed ‘holistic analysis’(Gross et al. 2014), was used in *Pan* and *Homo* whole bones or

epiphyses, but parameters were not used conjointly to discriminate functional groups in the statistical assessment either. It is noteworthy, however, that Tsegai et al. (2017), used the same method and performed a Principal Component Analysis. Skinner et al. (2015) and Stephens et al. (2016)) also used Gross et al. (2014)'s method, but focused on trabecular architecture only. This approach is particularly relevant for medium- to large-sized mammals such as *Pan* or *Homo*, for which the epiphyses include a complex trabecular architecture with distinct zones of different arrangement. One can note that an entirely different approach, not relying on the measurement of these parameters, but on micro-finite element analysis, was also applied to a primate (Huynh Nguyen et al. 2014). To our knowledge, epiphyseal trabecular and mid-diaphyseal parameters were never combined in a functional analysis about non-primate taxa, and no analysis used both trabecular and cross-sectional parameters in the same discriminant test.

As early as the 19th century, it was recognized that "ground sloths", *Megatherium* in particular (Owen 1861), were characterized by a medulla filled with spongy bone (see review of the matter by Amson and Nyakatura (2017). This feature was argued to be suited to withstand compression in this large-sized taxon (Blanco & Czerwonogora 2003). Compactness profile of a mid-diaphyseal section was studied in various extant and extinct xenarthrans by Straehl et al. (2013). They found that most armadillos were characterized by a humeral mid-diaphysis that is relatively more compact than that of the femur. Finally, Amson et al. (2017a) studied the epiphyseal trabecular architecture in extant xenarthrans, and found that some parameters, the degree of anisotropy (DA) in particular, differed among functional categories.

Indeed, xenarthrans are marked by distinct lifestyles that can be used to define functional categories. Extant xenarthrans were categorized by Amson et al. (2017a) as fully arboreal (extant sloths), intermediate (anteaters), and fully terrestrial and fossorial

(armadillos), and several fossorial classes were recognized among the latter. Those categories mostly match the phylogeny (i.e., most classes correspond to one clade). However, this is likely not true anymore, if one includes the extinct xenarthrans, the “ground sloths” in particular.

Lifestyle reconstruction of extinct xenarthrans dates back to the 18th century (see review by Amson and Nyakatura (2017)). Various methods were employed to infer the lifestyle of extinct xenarthrans. So far, they all relied on bone (and teeth) gross morphology, involving approaches such as biomechanical modelling (Fariña & Blanco 1996) or muscle reconstruction (Toledo et al. 2013). This was found as challenging, partly because of the lack of modern analogues for some taxa (Vizcaíno et al. 2017), and partly because of the autapomorphic nature of several of the xenarthran traits (including that of extant taxa), which makes disentangling the phylogenetic and functional signals difficult (Amson et al. 2017a). Bone structure was argued to be extremely plastic in general, and found, in xenarthrans in particular, to be mostly devoid of phylogenetic signal (and when a significant signal is found, it is likely due to the matching between functional categories and clades (Amson et al. 2017a)). The ecophenotypic character of bone structure (Ryan et al. 2018) is the rationale behind the present endeavour.

Extant sloths represent but a remnant of the overall diversity of Tardigrada, and most likely acquired their highly derived lifestyle convergently (Nyakatura 2012; Coutier et al. 2017). The fossil record of early (Palaeocene-Eocene) xenarthrans and especially that of sloths, is rather poor (Gaudin & Croft 2015). It is therefore hard to reconstruct the ancestral lifestyle of Tardigrada, and more generally Xenarthra. To date, no extinct sloths have been reconstructed to have had a suspensory posture and locomotion resembling their extant kin. But, because their gross anatomy was considered as similar to that of extant anteaters, Matthew (1912) argued that *Hapalops*, for instance, was partly arboreal. Such lifestyle was of

course not considered for larger taxa (but see translation of Lund in Owen (1839) for an early opposite view). However, digging capabilities, as well as bipedal stance and/or locomotion, was proposed for several medium-sized (e.g., *Glossotherium*) to giant-sized (e.g., *Megatherium*) "ground sloths" (Bargo et al. 2000; Patiño & Fariña 2017). For the present analysis, we were able to sample small-sized as well as large-sized "ground sloths." The estimated body sizes of the latter exceed that of extant xenarthrans by an order of magnitude (see below for body mass estimates). Because this has already been pointed out as a challenge for the reconstruction of extinct xenarthrans' lifestyles (Vizcaíno et al. 2017), and because size might be correlated to at least some bone structure parameters, our approach also identified potential challenges inherent to the taxa and parameters we studied.

Material and Methods

Specimen and scanning procedure

The dataset of Amson et al. (2017a), which consists of extant skeletally mature wild-caught xenarthrans, was extended by several extinct sloths roughly spanning the whole body size range of the group: the small-sized (ca. 38 kg (Bargo et al. 2012)) *Hapalops* sp., Ameghino, 1887 (Santa Cruz Formation, Early Miocene, ca. 17 Ma (Perkins et al. 2012)), the medium-sized *Valgipes bucklandi* (ca. 200 kg (Smith et al. 2003); Lagoa Santa, Brazil, Pleistocene; the sampled specimen MNHN.F.BRD29 is labelled *Ocnopus gracilis*, which is now viewed as a junior synonym (Cartelle et al. 2009)) and *Glossotherium robustum* (ca. 1200 kg (Vizcaíno et al. 2006); 'Pampean', Argentina and Tarija, Bolivia, both Pleistocene), and the large-sized *Lestodon armatus* (ca. 3200 kg (Vizcaíno et al. 2006); 'Pampean', Argentina, Pleistocene) and *Megatherium americanum* (ca. 4000 kg (Fariña et al. 1998); 'Pampean', Argentina, Pleistocene). All fossils were scanned (micro computed tomography, µCT) using a v|tome|x 240 L system (GE Sensing & Inspection Technologies Phoenix X|ray)

at the AST-RX platform of the Museum national d'Histoire naturelle (Paris, France; http://www.ums2700.mnhn.fr/ast-rx/ressources). According to the methodology and results of Amson et al. (2017a), we focused our data acquisition of the trabecular parameters on the humeral head and radial trochlea regions of interest (ROIs; see below). Mid-diaphyseal parameters were acquired for these two bones and for the third metacarpal (Mc III) in all species, when available. See Table 1 for the list of skeletal elements sampled for each extinct species, along with ROIs for which data were successfully acquired. For the included specimens, scanning resolution ranged from 0.03 to 0.123µm (depending on the size of the specimens). Relative resolution, used to assess if the employed resolution is adequate to analyse trabecular bone (mean trabecular thickness divided by resolution) ranged from 5.1 to 11.5 pixels/trabecula. This is considered as appropriate (Sode et al. 2008; Kivell et al. 2011; Mielke et al. 2018). For this first endeavour of palaeobiological reconstruction of "ground sloths" lifestyle based on bone diaphyseal and trabecular structure, we compared the parameters yielded by the fossils to those of the extant specimens, using the same lifestyle categories as defined by Amson et al. (2017a), i.e., the fully arboreal sloths, intermediate anteaters, and fully terrestrial and fossorial armadillos.

Qualitative observation of the diaphyseal structure

Raw image stacks were visualized with the Fiji package (ImageJ2 v. 1.51n and plugins (Schindelin et al. 2012, 2015; Schneider et al. 2012)). The routine 'Orthogonal views' was used to compute longitudinal sections. Sedimentary matrix prevented satisfying segmentation for some specimens but at least some qualitative observations were possible for all specimens (see Table 1).

Trabecular parameters

We followed the methodology of Amson et al. (2017a), which involves the use of the BoneJ plugin (Doube et al. 2010) for Fiji. In brief, bones were placed in the same standard orientation, ROIs were selected in the centre of the studied epiphyses (to be as large as possible but without including cortical bone), the resulting substack was thresholded ('Optimise Threshold> Threshold Only' routine), purified ('Purify' routine), and trabecular parameters were measured. Given the results of Amson et al. (2017a), we focused on the degree of anisotropy (DA), main direction of the trabeculae (MDT), bone volume fraction, BV/TV, connectivity density (Conn.D), trabecular mean thickness (Tb.Th), trabecular mean spacing (Tb.Sp), bone surface area (BS). Other trabecular parameters routinely acquired, however, can also be found in Supplementary Online Material (SOM) 1.

For some specimens, the lack of contrast between bone and the sedimentary matrix prevented accurate bone segmentation (see Table 1). Thresholding (see above) was successfully performed for the rest of the specimens; some of the latter, however, required manual removal of a few sedimentary particles (using the un-thresholded stack to recognize them).

The humerus of two specimens of *Hapalops* showed a slight remnant of epiphyseal line. A smaller ROI was hence defined to exclude this line (which would have biased the measurements) by cropping isometrically (in 3D) the substack (custom ImageJ script, SOM 2). The cropping coefficient (MNHN.F.SCZ162: 39%; MNHN.F.SCZ164: 72%) was then applied to the whole dataset and trabecular parameters were acquired anew. The means of the latter were compared to the initial parameters. For the dataset cropped at 72%, differences were found as minor (similar MDT; ΔDA = 3%; ΔBV/TV < 1%; ΔConnD <1%), while for the dataset cropped at 39%, differences were more important (MDT of opposing direction; ΔDA, 13%; ΔBV/TV = 2%; ΔConnD, 4%). We hence did not analyse further the latter dataset (and excluded MNHN.F.SCZ162 from the analysis of trabecular architecture). A remnant of

epiphyseal line was also observed in *Glossotherium robustum* MNHN.F.PAM756, but in its case only qualitative observations were made.

Mid-diaphyseal parameters

The same standardly oriented µCT-scan stacks (see above) were used for the acquisition of mid-diaphyseal parameters. Using Fiji, a cross-section was selected at mid-diaphysis; the latter was defined as the midpoint between most proximal and most distal points of either articular surfaces. Several sampled fossils did not preserve the mid-diaphysis. To compare them to the rest of the specimens, the latter were re-sampled at the level closest to mid-diaphysis preserved by each of those fossils (as assessed by superimposition with a complete specimen of the same species; MNHN.F.CSZ164 (humerus): 35% from proximal end; MNHN.F.CSZ166 (radius): 72% from the proximal end; see Table 1). Once the mid-diaphyseal cross-sections were selected, they were thresholded automatically (see above), but we manually checked the resulting image, which, in a few instances, required a manual correction of the levels. The whole sectional area (WArea), global compactness (both acquired with a custom ImageJ script, SOM 3), and cross-sectional parameters of the 'Slice Geometry' routine of BoneJ (Doube et al. 2010) were acquired. For the following analyses, we focused on cross-sectional area (CSA) and the ratio of second moment of area around major to minor axes (Imax/Imin), also termed cross-sectional shape (CSS). If the ratio is close to one, CSS will usually be roughly circular. Values above one will entail increasingly elliptical shapes. The other trabecular parameters, however, can also be found in SOM 1. Because it is redundant with GC, CSA will only be used as a potential body size proxy (see below).

Statistics

The whole statistical analysis was performed using R version 3.4.3. Amson et al. (2017a) accounted for size effects by computing a phylogenetically informed linear regression for each parameter, against a size proxy. If the regression was found as significant, its residuals were used as the 'size-corrected' parameter. But the size of "ground sloths", well exceeding for most of them that of extant xenarthrans, could bias such a procedure. Indeed, the slightest error on the regression coefficients estimation would likely involve drastically different residuals for those outlying taxa (see also Discussion). We therefore favoured, for the present analysis, to normalize those parameters that have a dimension by dividing the trait value by a body size proxy (raised to the same dimension). As body size proxies, we considered the specimen-specific TV (for trabecular parameters) and WArea (mid-diaphyseal parameters) or body mass (BM; specific averages, because unknown for most collection specimens). Specific body masses were taken from the AnAge database (Tacutu et al. 2013) and additional sources when necessary (Vizcaíno et al. 1999; Hayssen 2010; Abba & Superina 2016; Smith & Owen 2017) for the extant species and from the specific sources mentioned above for the extinct. The coefficient of determination of regressions against a parameter well known to correlate with size (Tb.Th for trabecular parameters and CSA for mid-diaphyseal parameters) indicated that BM was more representative of the sample variance for the trabecular parameters, while it was WArea in the case of mid-diaphyseal parameters. They were accordingly used as body size proxies in the subsequent analyses.

The timetree used by Amson *et al* (2017a) (which is based on Gibb et al. (2016)) was completed with the extinct taxa. The relationships between the main clades follow Amson et al. (2017b). The split between Mylodontidae (represented by *Lestodon*) and the other Eutardigrada (all sloths but *Bradypus*) was set according to the age of the oldest fossil pertaining to the clade (*Octodontotherium*, ca. 29 Ma (Flynn, Swisher, 1995 in Kay et al., 1998) and is thus conservative (Fig. 1). The age of divergence between *Lestodon* and

Glossotherium was set according to the age of *Thinobadistes* (Hemphillian, ca. 9 Ma (Woodburne 2010)), which is more closely related to *Lestodon* than *Glossotherium* according to Gaudin (2004). Extinct sloths were placed according to their known geological ages (see above; for Pleistocene taxa, a relatively young age of 0.1 Ma was arbitrarily given. Length of the branches leading to nodes of unknown ages, which are in direct relation to extinct taxa, and from these to terminal extinct taxa, were arbitrarily set at 1 and 0.1 Ma, respectively.

Beside univariate comparisons, we performed linear discriminant analyses to infer the most likely lifestyle of extinct species. Both trabecular and mid-diaphyseal parameters of the humerus and radius were conjointly used in these analyses (parameters from the Mc III were not included because of their lack of discrimination power, see Results). To account for the great body size disparity of the studied taxa, it is the 'size-normalized' parameters that were used (raw value divided by the relevant body size proxy if parameter not dimensionless, see above). One analysis per extinct taxon was performed, because we were not able to acquire all parameters for each of them (depending on the successfully processed skeletal elements and ROIs, see Table 1). To phylogenetically inform these analyses, we used the function pFDA (Motani & Schmitz 2011; latest version available on github.com/lschmitz/phylo.fda). This 'phylogenetic flexible discriminant analysis' uses the optimised value of Pagel's Lambda to account for the phylogenetic signal (Pagel 1999). As implemented here, the latter can span from 0 to 1, respectively denoting absence of phylogenetic signal and trait evolution consistent with a Brownian motion model of evolution. In the case of *Hapalops*, the number of parameters exceed that of included taxa, and the most likely Lambda could not be successful retrieved. Dimension number was hence reduced by using the first PCs of a PCA (excluding the last two out of 17 PCs was enough to recover the most likely Lambda; the first 15 PCs represented 99% of the variance). The rest of the pFDA works as a 'traditional' discriminant analysis, with training data (in our case that of the extant armadillos, anteaters,

and sloths) and test data (in our case that of the extinct sloths). If not normally distributed (as indicated by a Shapiro test), the parameters were log-transformed.

Institutional abbreviations

MCL, Museu de Ciencias Naturais da Pontifícia Universidade Católica de Minas Gerais, Belo Horizonte, Brazil; **MNHN.F**, Muséum national d'Histoire naturelle, Paris, France, Palaeontology collection; **ZMB_MAM**, Museum fu□r Naturkunde Berlin (Germany), Mammals Collection; **ZSM**; Zoologische Staatssammlung Mu□nchen, Germany.

Results

Qualitative observations of diaphyseal structure

In the humerus of small armadillos and anteaters, the medullary cavity is mostly devoid of spongy bone (with just a few isolated trabeculae, e.g., *Chaetophractus vellerosus* ZSM-1926-24, Fig. 2A; *Cyclopes didactylus*, ZMB_MAM_3913). In larger members of these clades, the medullary cavity is filled throughout the proximodistal length of the diaphysis by a more or less dense spongiosa (e.g., *Priodontes maximus* ZSM-1931-293; *Myrmecophaga tridactyla*, ZMB_MAM_102642; Fig. 2B-C). In extant sloths, a spongiosa can be observed in most of the diaphysis (*Bradypus*; n=4) or throughout its length (*Choloepus*, Fig. 2E; n=4), but a central region free of trabeculae subsists. The medullary cavity of the whole diaphysis is full of spongy bone in *Glossotherium* (n=1; Fig. 2F). It is nearly full in *Scelidotherium*, with just a small central free region subsisting (n=1). For *Hapalops*, a clear assessment cannot be given due to the preservation of the specimens at hand (MNHN.F.SCZ162 seems to show a free medullary cavity, but MNHN.F.SCZ164, which only preserves the proximal third of bone, shows a medullary cavity full of spongy bone). The whole diaphysis of the larger sloths

Megatherium and *Lestodon* were not observed, but it is noteworthy that their epiphyses are filled with dense spongiosa (each n=1).

The radius of extant xenarthrans shows the same pattern as the humerus. In *Glossotherium*, *Lestodon*, and *Megatherium*, the medullary cavity of the whole radial diaphysis is essentially full of spongy bone (Fig. 2G; no data for *Hapalops* for which the entire radial epiphysis could not have been sampled). While the hind limb was not sampled for this study, it is noteworthy that the observation of a 'naturally sectioned' tibia of the small-sized *Nothrotherium* reveals that the medullary cavity is entirely filled with dense spongy bone (Fig. 2D).

Univariate comparisons

The structure of the Mc III of extant species did not differ notably among the lifestyle categories (Fig. 3A-B). There is only a tendency for the anteaters and armadillos to have a more compact mid-diaphysis (Fig. 3A). Mc III structure was therefore not further studied, and not included in the discriminant analyses (see below). One can note, however, that some armadillos have an outlyingly high CSS (i.e., very elliptic cross-section) at mid-diaphysis (Fig. 3B; the single most elliptic value is found in the subterranean *Calyptophractus retusus* ZSM-1961-316). A great disparity of CSS at this location is found in extinct sloths, with the value of *Valgipes* falling among the outlying armadillos just mentioned, and that of *Megatherium* being the single lowest (i.e., most circular cross-section).

The humeral diaphysis in *Hapalops* is remarkably compact. At mid-diaphysis (n=1), it features the highest GC value of the whole dataset (Fig. 3C). At 35% of the diaphyseal length (from the proximal end; n=2), *Hapalops* falls in the uppermost distribution of the extant sloths. The CSS at humeral mid-diaphysis of *Hapalops* falls among the low values (i.e., round cross-section) of extant sloths (Fig. 3D), but among those of anteaters at 35% of the

diaphyseal length. In *Scelidotherium* (n=1), the GC of the humerus at mid-diaphysis is higher than that of most extant xenarthrans, falling in the upper distribution of armadillos and extant sloths (Fig. 3C). One should note, however, that this parameter does not yield any clear distinction among lifestyles. The humeral CSS at mid-diaphysis of *Scelidotherium*, on the other hand, falls among anteaters (Fig. 3D).

The radial diaphysis of *Hapalops* features a GC value (n=1; sampled at 72% of diaphyseal length) that falls among the distribution of armadillos, being slightly higher than extant sloths' values. The GC of *Glossotherium* and *Lestodon* at radial mid-diaphysis is very low, which agrees with the tendency observed in extant sloths (Fig. 3E). Their high CSS (i.e., more elliptical section), however, falls beyond the distribution of most extant xenarthrans, being only tied or exceeded by two outlying armadillos (Fig. 3F).

Regarding the trabecular architecture parameters, only the degree of anisotropy (DA) will be presented with univariate comparisons, as it was singled out as the most functionally informative of these parameters in extant xenarthrans (Amson et al. 2017a). For the humeral head, using a ROI representing 72% of the maximum volume (see Material ad Methods section), both *Hapalops* and *Lestodon* (n =1 in each case) fall in the upper distribution (i.e., more anisotropic) of extant sloths and anteaters, which tend to feature lower values than the armadillos (Fig. 4A). The same pattern is found for the full ROI in *Lestodon* (no data for *Hapalops*, see Material ad Methods section). In the distal radius (trochlea), the DA value of *Hapalops* falls above the main distribution of extant sloths, within that of anteaters (Fig. 4B). *Glossotherium* is the sampled taxon with the single lowest DA value (most isotropic structure). One should note, however, that DA was significantly correlated to body size (see Discussion). The main direction of the trabeculae (MDT) in the radial trochlea (humeral head did not yield lifestyle discrimination; Amson et al. 2017b) of both *Hapalops* and

Glossotherium falls outside the distribution of extant xenarthrans (Fig. 4C). In both cases, the MDT falls closer to the distribution of extant sloths.

Phylogenetically flexible discriminant analyses

For *Hapalops*, 18 parameters could have been included in the analysis (diaphyseal and trabecular parameters, from both the humerus and radius), of which the dimensionality was reduced with a PCA (see Material and Methods section). The recovered optimal Lambda is 0.39 and the discrimination is optimal (training misclassification error of 0%). *Hapalops* is classified as a sloth with a high posterior probability (>99%). However, it clearly falls beyond the distribution of extant xenarthrans (Fig. 4A).

For *Lestodon*, eight parameters could have been included (from the radial diaphysis and humeral head trabeculae). The recovered optimal Lambda is 0.80, and training misclassification error is 38%. It is classified as an anteater with a rather low posterior probability (68%), the second most probable classification being to armadillos (32%). According to this analysis, a classification as a sloth is very improbable (0.03%). *Lestodon* falls beyond the distribution of extant xenarthrans (Fig. 4B).

For *Glossotherium*, eight parameters could have been included (from the radial diaphysis and trabeculae of the radial trochlea). The recovered optimal Lambda is 0.88, and training misclassification error is 35%. The most probable classification is to anteaters (50%), followed by the equally probable classifications to armadillos or sloths (each 25%). *Glossotherium* falls within the distribution of extant xenarthrans, but outside the distribution of each lifestyle class, just outside that of anteaters (Fig. 4C).

For *Scelidotherium*, only two parameters could have been included (from the humeral diaphysis). An optimal Lambda of 0.96 and a high training misclassification error of 69% were recovered. The three possible classifications are roughly equally likely (anteater: 37%;

sloth: 36%; armadillo: 27%). *Scelidotherium* basically falls in the middle of the distribution of extant xenarthrans (Fig. 4D).

Discussion

On the whole, the classification of extinct sloths to one of the extant xenarthran lifestyles (that of armadillos, anteaters, or extant sloths) based on forelimb bone structure proved to be challenging. This appears to be due to at least three obvious causes: (1) the imperfect lifestyle discrimination based on diaphyseal and trabecular parameters, (2) the difficulties raised by the size correction (for some parameters), and (3) the fact that the values of extinct taxa are outliers with respect to the distribution of extant xenarthrans (for some parameters).

The four discriminant analyses we performed vary greatly in the number of included parameters. As expected, analyses including more parameters yielded a better discrimination. The lowest misclassification error (0%) was obtained for the analysis of *Hapalops*, for which it was possible to include 15 parameters (18 before dimension reduction) from both the diaphysis and epiphyseal trabeculae. The worst discrimination (69% of misclassification error) was found for the analysis of *Scelidotherium*, for which only two parameters, from the humeral diaphysis, could have been included. This lends support to the approach of including parameters from several bone compartments, if one endeavours to discriminate lifestyles based on these parameters.

Several of the investigated parameters were significantly correlated to body size. To attempt to prevent the size of the studied taxa to influence the analysis, a common approach is to size-correct the raw data using the residuals of a regression of the trait against a body size proxy (Mccoy et al. 2006). This proved to be challenging for extinct sloths, because, for most of them, body size largely exceeds that of extant xenarthrans (Vizcaíno et al. 2017). This

potentially makes the size regressions spurious, as the extreme values over-influence the regression coefficients. This is not a trivial consideration for our dataset. For instance, if one would size-correct the DA in the radial trochlea using the residuals of the corresponding size regression, the medium-sized extinct sloth *Glossotherium*, of which the raw DA value was found as the lowest of the dataset, would fall in the middle of the overall distribution. For those parameters that are dimensionless, we hence decided to use the untransformed data. But this is likely to be biased as well. For instance, the scaling exponent of the degree of anisotropy (DA) across Mammalia in the femoral head or condyle was found by Doube et al. (2011) as negative (95% confidence interval excluded 0; the reported p-value however was higher than 0.05). We also found a negative scaling exponent for one of the investigated ROI, the radial trochlea (which was in our case found as significant). It would be suboptimal to exclude this parameter, especially because it was found as the best functionally discriminating parameter in extant xenarthrans (Amson et al. 2017a). It was also singled out as reflecting joint loading in primates better than other parameters (Tsegai et al. 2018). A way to make the size-correction more accurate in our case would be to include xenarthrans to the sampling that have a body size between that of extant species and that of the giant “ground sloths”, i.e., with a mass roughly between 50 kg and 300 kg. Unfortunately, the number of known xenarthrans of this size range is very limited.

It was already obvious from univariate comparisons that the bone structure in *Hapalops*, the small-sized extinct sloth, departed from the condition observed in extant xenarthrans. Indeed, the overall great compactness of its humeral diaphysis does not seem to be matched by any other sampled xenarthrans (but see aquatic specialization of *Thalassocnus* (Amson et al. 2014). This does not seem to be a systemic bone mass increase (Amson et al. 2018), because neither the trabecular parameters nor the compactness of the radial diaphysis of this taxon seems to be notably affected by bone mass increase. Finding a compact humerus

is particularly surprising, as the stylopod can be expected to be less compact in terrestrial mammals (Amson & Kolb 2016). In the case of *Lestodon*, it was not obvious from univariate comparisons that its bone structure was outlying, but both the latter and *Hapalops* fell outside the range of extant xenarthrans in the respective discriminant analyses. One may hence conclude that, based on their bone structure, the humerus and radius of both *Hapalops* and *Lestodon* were likely involved in a loading regime different from those associated with the lifestyles of extant xenarthrans. For *Hapalops*, one can however note that the phylogenetically informed discriminant analysis strongly supports a classification as an extant sloth, which indicate that some features of their mechanical environment might have been similar. The main direction of the trabecular (MDT) also agrees with the fact that the bone structure of extant sloth is different but the most similar of the three extant lifestyles (Fig. 4C). Based on bone gross morphology, *Hapalops* was previously reconstructed as partly or primarily arboreal (Matthew 1912; White 1997). Both bone structure and gross morphology therefore seem to point in the same direction for the reconstruction of *Hapalops*' lifestyle. The large-sized *Lestodon*, on the other hand, is not classified with strong support to one of the extant groups. The least probable classification is to extant sloths (0.03% of posterior probability), which might suggest that the bone structure of *Lestodon* resembles more that of anteaters and armadillos. Naturally, suspensory posture was never purported for this elephant-sized sloth. *Lestodon* was interpreted as traviportal (slow-moving with both quadrupedal and bipedal stances) by Toledo (1996), and the forelimb gross morphology was found as consistent with a fossorial activity (but probably not to procure food (Coombs 1983); see Bargo et al. (2000) for a more tempered interpretation). Including other fossorial and non-fossorial taxa to the sampling of the bone structure analysis will be necessary to suggest a more precise assertion regarding the digging habits of this taxon (but its large size will be problematic, see above). The two other extinct sloths subject to a discriminant analysis, *Glossotherium* and

Scelidotherium, differ from the former two in falling within the distribution of extant xenarthrans. However, in neither case the classification is clear, and it seems that acquiring more of their bone structure parameters will be necessary to draw reliable conclusions.

The Mc III did not yield clear discrimination among the extant lifestyles and was hence not included in the discriminant analyses. But one can note that an interesting pattern was observed in the cross-sectional shape (CSS) of extinct sloths at mid-diaphysis. Indeed, high values, denoting elliptic sections, are found in *Valgipes* and *Glossotherium*. Such a bone structure is expected to be suited to resist bending along its major axis (Ruff & Hayes 1983). This is consistent with previous lifestyle reconstruction of *Glossotherium*, which is argued to have had fossorial habits (Coombs 1983; Bargo et al. 2000) supposedly entailing a well-marked main direction of bending. Furthermore, it might suggest that *Valgipes* had similar habits, which, to our knowledge, was never purported.

It has been repetitively argued that the medulla filled with spongy bone observed in large-sized xenarthrans has a functional significance (see review of Amson and Nyakatura (2017)). This was more generally suggested for large-sized mammals, and argued as a potential adaptation to graviportality (Houssaye et al. 2015). It does not seem to be possible to easily draw such a conclusion for xenarthrans: whatever their lifestyle, xenarthrans with a mass of roughly 5 kg (e.g., *Tamandua*) and over tend to fill their medullary cavity with spongy bone. This is true for the forelimb, as described here (and as also reported by Houssaye et al. (2015) for the humerus), but likely also for the hind limb, as suggested by the tibia of the small-sized extinct sloth *Nothrotherium* (ca. 80 kg) described herein. In the case of xenarthrans, the great quantity of diaphyseal trabeculae might be related to another aspect affecting bone structure, such as mineral homeostasis and/or metabolism.

The extremely low metabolism of extant sloths was suggested by Montañez et al. (under review) as a potential explaining factor for their low cortical compactness (CC).

Indeed, they found that extant sloths depart in that regard from other extant xenarthrans as well as from two extinct sloths (the small-sized *Hapalops* and *Parocnus*). No quantitative assessment of CC was performed here. But we can report that, at mid-diaphysis, the CC of the sampled extinct sloths was generally observed as low (when it could have been observed), as in armadillos and anteaters. Nevertheless, two specimens showed a rather porous cortex, *Hapalops* (humerus; MNHN.F.SCZ162) and *Glossotherium* (radius; MNHN.F.PAM756), though not as porous as that of most extant sloths. A dedicated analysis of extinct sloths' CC is required to investigate this trait and possibly use it to inform metabolic rate reconstruction in extinct sloths.

Conclusion

Bone structure of the diaphysis and epiphyses of the third metacarpal, humerus, and radius was here investigated in several species of extinct sloths, comparing it to that of extant xenarthrans. Related parameters were successfully acquired and included in phylogenetically flexible discriminant analyses. The latter constitute, to our knowledge, the first analyses that conjointly include both diaphyseal and trabeculae parameters to discriminate lifestyles. The identified challenges were the lack of discrimination power of some parameters, the difficulties raised by size-correlated parameters, and the fact that some parameters fall outside the range described by extant taxa. As a result, no extinct sloths are here confidently ascribed to one of the lifestyles of extant xenarthrans. The humeral and radial structure of the small-sized *Hapalops*, from the Miocene of Argentina, was nevertheless found as more reminiscent of that of extant sloths, which agrees with the conclusions drawn based on gross morphology. The humeral and radial structure of the large-sized *Lestodon*, from the Pleistocene of Argentina, clearly departs from that of extant sloths. The singular bone structure of xenarthrans, including a medullary cavity filled with spongy bone in most taxa, and a low

cortical compactness in extant sloths, deserves further investigations. Because Xenarthra is argued to be one of the major clades of placental mammals (Asher et al. 2009; Gaudin & Croft 2015), such investigations are not only important for the understanding of the evolutionary history of the clade, but potentially for that of Mammalia as well.

Acknowledgements

We warmly thank the following curators and collection managers: Guillaume Billet (Muséum national d'Histoire naturelle, Paris; MNHN), Cástor Cartelle (Museu de Ciencias Naturais da Pontifícia Universidade Católica de Minas Gerais, Belo Horizonte, Brazil), Anneke H. van Heteren (Zoologische Staatssammlung München), Frieder Mayer and Christiane Funk (Museum für Naturkunde Berlin), Thomas Kaiser and Nelson Ribeiro Mascarenhas (Universität Hamburg), Irina Ruf and Katrin Krohmann (Senckenberg Forschungsinstitut und Naturmuseum), Stefan Merker (Staatlichen Museums für Naturkunde Stuttgart), Eva Bärmann (Zoologische Forschungsmuseum Alexander Koenig). Anneke H. van Heteren (Zoologische Staatssammlung Mu□nchen), Patrick Arnold (Friedrich-Schiller-Universita□t Jena), and Aurore Canoville (NC State University) are acknowledged for helping with acquisition of the extant species scans. We thank Patricia Wills, Marta Bellato, and Maïté Adam (AST-RX platform, MNHN) for acquiring the extinct species scans. This research received support from the SYNTHESYS Project http://www.SYNTHESYS.info/ which is financed by European Community Research Infrastructure Action under the FP7 Integrating Activities Programme. EA was funded by the Alexander von Humboldt Foundation. JAN and EA were funded by the German Research Council (DFG EXC 1027 and DFG AM 517/1-1, respectively).

Authors' contributions

Conceptualization and methodology, EA, JAN; Formal analysis, EA; Investigation, EA; Writing – Original draft, EA; Writing – Review & editing, EA, JAN. All authors gave final approval for publication.

References

Abba, A. M., and M. Superina. 2016. *Dasypus hybridus* (Cingulata: Dasypodidae). Mammalian Species 48:10–20.

Amson, E., P. Arnold, A. H. van Heteren, A. Canoville, and J. A. Nyakatura. 2017a. Trabecular architecture in the forelimb epiphyses of extant xenarthrans (Mammalia). Frontiers in Zoology 14:52.

Amson, E., G. Billet, and C. de Muizon. 2018. Evolutionary adaptation to aquatic lifestyle in extinct sloths can lead to systemic alteration of bone structure. Proceedings of the Royal Society B 285:20180270.

Amson, E., and C. Kolb. 2016. Scaling effect on the mid-diaphysis properties of long bones—the case of the Cervidae (deer). The Science of Nature 103:58.

Amson, E., C. de Muizon, and T. J. Gaudin. 2017b. A reappraisal of the phylogeny of the Megatheria (Mammalia: Tardigrada), with an emphasis on the relationships of the Thalassocninae, the marine sloths. Zoological Journal of the Linnean Society 179:217–236.

Amson, E., C. de Muizon, M. Laurin, C. Argot, and V. de Buffrénil. 2014. Gradual adaptation of bone structure to aquatic lifestyle in extinct sloths from Peru. Proceedings of the Royal Society B: Biological Sciences 281.

Amson, E., and J. A. Nyakatura. 2017. The postcranial musculoskeletal system of Xenarthrans: Insights from over two centuries of research and future directions. Journal of Mammalian Evolution, doi: 10.1007/s10914-017-9408-7.

Asher, R. J., N. Bennett, and T. Lehmann. 2009. The new framework for understanding placental mammal evolution. BioEssays 31:853–864.

Barak, M. M., D. E. Lieberman, and J.-J. Hublin. 2011. A Wolff in sheep's clothing: Trabecular bone adaptation in response to changes in joint loading orientation. Bone 49:1141–1151.

Barak, M. M., D. E. Lieberman, D. Raichlen, H. Pontzer, A. G. Warrener, and J. J. Hublin. 2013. Trabecular evidence for a human-like gait in *Australopithecus africanus*. PLoS ONE 8.

Bargo, M. S., N. Toledo, and S. F. Vizcaíno. 2012. Paleobiology of the Santacrucian sloths and anteaters (Xenarthra, Pilosa). Pp. 216–242 *in* S. F. Vizcaíano, R. F. Kay, and M. S. Bargo, eds. Early Miocene Paleobiology in Patagonia: High-Latitude Paleocommunities of the Santa Cruz Formation. Cambridge University Press, Cambridge.

Bargo, M. S., S. F. Vizcaíno, F. M. Archuby, and R. E. Blanco. 2000. Limb bone proportions, strength and digging in some Lujanian (late Pleistocene-early Holocene) mylodontid ground sloths (Mammalia, Xenarthra). Journal of Vertebrate Paleontology 20:601–610.

Blanco, R. E., and A. Czerwonogora. 2003. The gait of *Megatherium* Cuvier 1796. Senckenbergiana Biologica 83:61–68.

Cartelle, C., G. De Iuliis, and R. L. Ferreira. 2009. Systematic revision of tropical Brazilian scelidotheriine sloths (Xenarthra, Mylodontoidea). Journal of Vertebrate Paleontology 29:555–566.

Coombs, M. C. 1983. Large mammalian clawed herbivores: a comparative study. Transactions of the American Philosophical Society, New series 73:1–96.

Coutier, F., L. Hautier, R. Cornette, E. Amson, and G. Billet. 2017. Orientation of the lateral semicircular canal in Xenarthra and its links with head posture and phylogeny. Journal of Morphology 278.

DeSilva, J. M., and M. J. Devlin. 2012. A comparative study of the trabecular bony architecture of the talus in humans, non-human primates, and *Australopithecus*. Journal of Human Evolution 63:536–551.

Doube, M., M. M. Kłosowski, I. Arganda-Carreras, F. P. Cordelières, R. P. Dougherty, J. S. Jackson, B. Schmid, J. R. Hutchinson, and S. J. Shefelbine. 2010. BoneJ: Free and extensible bone image analysis in ImageJ. Bone 47:1076–1079.

Doube, M., M. M. Klosowski, A. M. Wiktorowicz-Conroy, J. R. Hutchinson, and S. J. Shefelbine. 2011. Trabecular bone scales allometrically in mammals and birds. Proceedings of the Royal Society B: Biological Sciences 278:3067–73.

Fariña, R. A., and R. E. Blanco. 1996. *Megatherium*, the stabber. Proceedings of the Royal Society B 263:1725–1729.

Fariña, R. A., S. F. Vizcaíno, and M. S. Bargo. 1998. Body mass estimations in Lujanian (late Pleistocene-early Holocene of South America) mammal megafauna. Mastozoología Neotropical 5:87–108.

Gaudin, T. J. 2004. Phylogenetic relationships among sloths (Mammalia, Xenarthra, Tardigrada): the craniodental evidence. Zoological Journal of the Linnean Society 140:255–305.

Gaudin, T. J., and D. A. Croft. 2015. Paleogene Xenarthra and the evolution of South American mammals. Journal of Mammalogy 96:622–634.

Germain, D., and M. Laurin. 2005. Microanatomy of the radius and lifestyle in amniotes (Vertebrata, Tetrapoda). Zoologica Scripta 34:335–350.

Gibb, G. C., F. L. Condamine, M. Kuch, J. Enk, N. Moraes-Barros, M. Superina, H. N. Poinar, and F. Delsuc. 2016. Shotgun mitogenomics provides a reference phylogenetic framework and timescale for living xenarthrans. Molecular Biology and Evolution 33:621–642.

Gross, T., T. L. Kivell, M. M. Skinner, N. H. Nguyen, and D. H. Pahr. 2014. A CT-image-based framework for the holistic analysis of cortical and trabecular bone morphology. Palaeontologia Electronica 17:1–13.

Hayssen, V. 2010. *Bradypus variegatus* (Pilosa: Bradypodidae). Mammalian Species 42:19–32.

Houssaye, A., K. Waskow, S. Hayashi, A. H. Lee, and J. R. Hutchinson. 2015. Biomechanical evolution of solid bones in large animals: a microanatomical investigation. Biological Journal of the Linnean Society 117:350–371.

Huynh Nguyen, N., D. H. Pahr, T. Gross, M. M. Skinner, and T. L. Kivell. 2014. Micro-finite element (μFE) modeling of the siamang (*Symphalangus syndactylus*) third proximal phalanx: The functional role of curvature and the flexor sheath ridge. Journal of Human Evolution 67:60–75.

Kivell, T. L. 2016. A review of trabecular bone functional adaptation: what have we learned from trabecular analyses in extant hominoids and what can we apply to fossils? Journal of Anatomy 228:569–594.

Kivell, T. L., M. M. Skinner, R. Lazenby, and J.-J. Hublin. 2011. Methodological considerations for analyzing trabecular architecture: an example from the primate hand. Journal of anatomy 218:209–25.

Kolb, C., T. M. Scheyer, K. Veitschegger, A. M. Forasiepi, E. Amson, A. A. E. Van der Geer, L. W. Van den Hoek Ostende, S. Hayashi, and M. R. Sánchez-Villagra. 2015. Mammalian bone palaeohistology: A survey and new data with emphasis on island forms. PeerJ 2015.

Lazenby, R. A., D. M. L. Cooper, S. Angus, and B. Hallgrímsson. 2008. Articular constraint, handedness, and directional asymmetry in the human second metacarpal. Journal of Human Evolution 54:875–885.

Matthew, W. D. 1912. The ancestry of edentates: as illustrated by the skeleton of *Hapalops*, a tertiary ancestor of the ground sloths. American Museum Journal 12:300–303.

Mccoy, M. W., B. M. Bolker, C. W. Osenberg, B. G. Miner, and J. R. Vonesh. 2006. Size correction: Comparing morphological traits among populations and environments. Oec 148:547–554.

Mielke, M., J. Wölfer, A. H. van Heteren, E. Amson, and J. A. Nyakatura. 2018. Trabecular architecture in the sciuromorph femoral head: allometry and functional adaptation. Zoological letters.

Motani, R., and L. Schmitz. 2011. Phylogenetic versus functional signals in the evolution of form–function relationships in terrestrial vision. Evolution 65:2245–2257.

Nyakatura, J. A. 2012. The convergent evolution of suspensory posture and locomotion in tree sloths. Journal of Mammalian Evolution 19:225–234.

Owen, R. 1861. Memoir on the *Megatherium*, or giant ground-sloth of America (*Megatherium americanum*, Cuvier). Williams and Norgate, London.

Owen, R. 1839. Part I. Fossil Mammalia. P. 111 *in* The Zoology of the Voyage of HMS Beagle. Smith Elder and Co, London.

Pagel, M. 1999. Inferring the historical patterns of biological evolution. Nature 401:877–884.

Patiño, S. J., and R. A. Fariña. 2017. Ungual phalanges analysis in Pleistocene ground sloths (Xenarthra, Folivora). Historical Biology 29:1065–1075.

Perkins, M. E., J. G. Fleagle, M. T. Heizler, B. Nash, T. M. Bown, A. A. Tauber, and M. T. Dozo. 2012. Tephrochronology of the Miocene Santa Cruz and Pinturas Formations, Argentina. Pp. 23–40 *in* S. F. Vizcaíno, R. F. Kay, and M. S. Bargo, eds. Early Miocene Paleobiology in Patagonia: high-latitude paleocommunities of the Santa Cruz Formation. Cambridge University Press, Cambridge.

Ruff, C. B., and W. C. Hayes. 1983. Cross-sectional geometry of Pecos Pueblo femora and

tibiae-a biomechanical investigation: I. Method and general patterns of variation. American journal of physical anthropology 60:359–81.

Ruff, C. B., B. Holt, and E. Trinkaus. 2006. Who's afraid of the big bad Wolff?: "Wolff's law" and bone functional adaptation. American Journal of Physical Anthropology 129:484–498.

Ryan, T. M., K. J. Carlson, A. D. Gordon, N. Jablonski, C. N. Shaw, and J. T. Stock. 2018. Human-like hip joint loading in *Australopithecus africanus* and *Paranthropus robustus*. Journal of Human Evolution 1–13.

Schindelin, J., I. Arganda-Carreras, E. Frise, V. Kaynig, M. Longair, T. Pietzsch, S. Preibisch, C. Rueden, S. Saalfeld, B. Schmid, J.-Y. Tinevez, D. J. White, V. Hartenstein, K. Eliceiri, P. Tomancak, and A. Cardona. 2012. Fiji: an open-source platform for biological-image analysis. Nature Methods 9:676–682.

Schindelin, J., C. T. Rueden, M. C. Hiner, and K. W. Eliceiri. 2015. The ImageJ ecosystem: An open platform for biomedical image analysis. Molecular Reproduction and Development 82:518–529.

Schneider, C. A., W. S. Rasband, and K. W. Eliceiri. 2012. NIH Image to ImageJ: 25 years of image analysis. Nature Methods 9:671–675.

Shaw, C. N., and T. M. Ryan. 2012. Does skeletal anatomy reflect adaptation to locomotor patterns? Cortical and trabecular architecture in human and nonhuman anthropoids. American journal of physical anthropology 147:187–200.

Skinner, M. M., N. B. Stephens, Z. J. Tsegai, A. C. Foote, N. H. Nguyen, T. Gross, D. H. Pahr, J. Hublin, and T. L. Kivell. 2015. Human-like hand use in *Australopithecus africanus*. Science 347:395–399.

Smith, F. A., S. K. Lyons, S. K. M. Ernest, K. E. Jones, D. M. Kaufman, T. Dayan, P. A. Marquet, J. H. Brown, and J. P. Haskell. 2003. Body Mass of Late Quaternary

Mammals. Ecology 84:3403.

Smith, P., and R. D. Owen. 2017. *Calyptophractus retusus* (Cingulata: Dasypodidae). Mammalian Species 49:57–62.

Sode, M., A. J. Burghardt, R. A. Nissenson, and S. Majumdar. 2008. Resolution dependence of the mon-metric trabecular structure indices. Bone 42:728–736.

Stephens, N. B., T. L. Kivell, T. Gross, D. H. Pahr, R. A. Lazenby, J.-J. Hublin, I. Hershkovitz, and M. M. Skinner. 2016. Trabecular architecture in the thumb of *Pan* and *Homo*: implications for investigating hand use, loading, and hand preference in the fossil record. American Journal of Physical Anthropology 161:603–619.

Straehl, F. R., T. M. Scheyer, A. M. Forasiepi, R. D. E. MacPhee, and M. R. Sánchez-Villagra. 2013. Evolutionary patterns of bone histology and bone compactness in xenarthran mammal long bones. PLoS ONE 8:e69275.

Su, A., and K. J. Carlson. 2017. Comparative analysis of trabecular bone structure and orientation in South African hominin tali. Journal of Human Evolution 106:1–18.

Su, A., I. J. Wallace, and M. Nakatsukasa. 2013. Trabecular bone anisotropy and orientation in an Early Pleistocene hominin talus from East Turkana, Kenya. Journal of Human Evolution 64:667–677.

Tacutu, R., C. T. Craig, A. Budovsky, D. Wuttke, G. Lehmann, D. Taranukha, J. Costa, V. E. Fraifeld, and J. De Magalhães. 2013. Human Ageing Genomic Resources: Integrated databases and tools for the biology and genetics of ageing. Nucleic Acids Research 41:D1027–D1033.

Toledo, N., M. S. Bargo, and S. F. Vizcaíno. 2013. Muscular reconstruction and functional morphology of the forelimb of early Miocene sloths (Xenarthra, Folivora) of Patagonia. Anatomical record 296:305–325.

Toledo, P. M. 1996. Locomotor Patterns within the Pleistocene Sloths. PhD Thesis,

University of Colorado.

Tsegai, Z. J., M. M. Skinner, A. H. Gee, D. H. Pahr, G. M. Treece, J.-J. Hublin, and T. L. Kivell. 2017. Trabecular and cortical bone structure of the talus and distal tibia in *Pan* and *Homo*. American Journal of Physical Anthropology 163:784–805.

Tsegai, Z. J., M. M. Skinner, D. H. Pahr, J.-J. Hublin, and T. L. Kivell. 2018. Systemic patterns of trabecular bone across the human and chimpanzee skeleton. Journal of Anatomy 232:641–656.

Vizcaíno, S. F., M. S. Bargo, and G. H. Cassini. 2006. Dental occlusal surface area in relation to body mass, food habits and other biological features in fossil xenarthrans. Ameghiniana 43:11–26.

Vizcaíno, S. F., R. A. Fariña, and G. V. Mazzetta. 1999. Ulnar dimensions and fossoriality in armadillos. Acta Theriologica 44:309–320.

Vizcaíno, S. F., N. Toledo, and M. S. Bargo. 2017. Advantages and limitations in the use of extant xenarthrans (Mammalia) as morphological models for paleobiological reconstruction. Journal of Mammalian Evolution, doi: 10.1007/s10914-017-9400-2.

White, J. L. 1997. Locomotor Adaptations in Miocene Xenarthrans. Pp. 246–264 *in* R. F. Kay, R. H. Madden, R. L. Cifelli, and J. J. Flynn, eds. Vertebrate paleontology in the neotropics. The Miocene fauna of La Venta, Colombia. Smithsonian Institution Press, Washington.

Woodburne, M. O. 2010. The Great American Biotic Interchange: dispersals, tectonics, climate, sea level and holding pens. Journal of mammalian evolution 17:245–264.

Table

Table 1. List of fossils with type of data acquired for each bone.

Species	Specimen number	Data type		
		Humerus	Radius	Mc III
Hapalops sp.	MNHN.F.SCZ166	-	72%MD; 100%TA	-
Hapalops sp.	MNHN.F.SCZ164	35%MD; 72%TA; (39%TA)	-	-
Hapalops sp.	MNHN.F.SCZ162	50%MD; 35%MD; (39%TA)	-	-
Lestodon armatus	MNHN.F.PAM754	-	50%MD	
Lestodon armatus	MNHN.F.PAM755	-	-	50%MD
Lestodon armatus	MNHN.F.PAM95	100%TA	-	-
Glossotherium robustum	MNHN.F.PAM756	QO	50%MD; 100%TA	-
Glossotherium robustum	MNHN.F.PAM141	-	-	50%MD
Scelidotherium leptocephalum	MNHN.F.PAM236	50%MD	-	-
Valgipes bucklandi	MNHN.F.BRD29	-	-	50%MD
Megatherium americanum	MNHN.F.PAM753	-	-	50%MD
Megatherium americanum	MNHN.F.PAM758	-	QO	-

Footnotes: Abbreviations: 'n'-MD, mid-diaphyseal data, with 'n' the position of the sampled cross-section from the proximal end; 'n'-TA, trabecular architecture data, with 'n' the cropping coefficient that was used, if any (see Material and Methods section); QO, only qualitative observations were performed.

Figure Legends

Figure 1. Timetree depicting the time-calibrated phylogenetic relationships of the xenarthrans included in the phylogenetically flexible linear discriminant analyses. See Material and Methods section for the sources used to build the timetree.

Figure 2. Qualitative observations of diaphyseal structure in xenarthrans. Longitudinal sections of humeri (A-C, E-F, all from CT-scans), tibia (D, 'natural' section), and radius (G, from CT-scan). A, *Chaetophractus vellerosus* (ZSM 1926-24); B, *Priodontes maximus* (ZSM 1931-293); C, *Myrmecophaga tridactyla* (ZMB_MAM_77025); D, *Nothrotherium maquinense* (MCL 2821); E, *Choloepus didactylus* (ZMB_MAM_35825); F, *Glossotherium robustum* (MNHN.F.TAR 767); G, *Lestodon armatus* (MNHN.F.PAM 754). Scale bars: A-E, 1 cm; F-G, 10 cm.

Figure 3. Univariate comparisons of mid-diaphyseal parameters. A, Mc III Global Compactness (GC); B, Mc III cross-sectional shape (CSS); C, humeral GC; D, humeral CSS; E, radial GC; F, radial CSS. Thresholded mid-diaphyseal virtual sections are depicted for the extinct sloths. Abbreviations: ant, anteaters; arma, armadillos; Glos, *Glossotherium*; Hapa, *Hapalops*; Lest, *Lestodon*; Meg, *Megatherium*; Sce, *Scelidotherium*; sloth, extant sloths.

Figure 4. Univariate comparisons of trabecular anisotropy parameters. A, degree of anisotropy (DA) in the humeral head ROI, reduced at 72% of its maximum size (see Material and Methods section); B, DA in the radial trochlea; C, main direction of the trabeculae (MDT) in the radial trochlea. Abbreviations: ant, anteaters; arma, armadillos; Glos, *Glossotherium*; Hapa, *Hapalops*; sloth, extant sloths.

Figure 5. Phylogenetically flexible linear discriminant analyses using humeral and radial bone structure parameters. One analysis per extinct taxon (referred as of “unknown” class) was performed, because of the difference in the parameters that could be included (see Material and Methods section and Table 1). A, *Hapalops*; B, *Lestodon*; C, *Glossotherium*; D, *Scelidotherium*. Abbreviations: ant, anteaters; arma, armadillos; sloth, extant sloths. The size of extinct sloths’ representations gives a rough indication of their body sizes.

Supplementary Online Material

SOM 1. Raw data. Excel document, of which each spreadsheet corresponds to a sampled region.

SOM 2. ImageJ macro to crop isometrically a stack in 3D.

SOM 3. ImageJ macro to acquire mid-diaphyseal parameters.

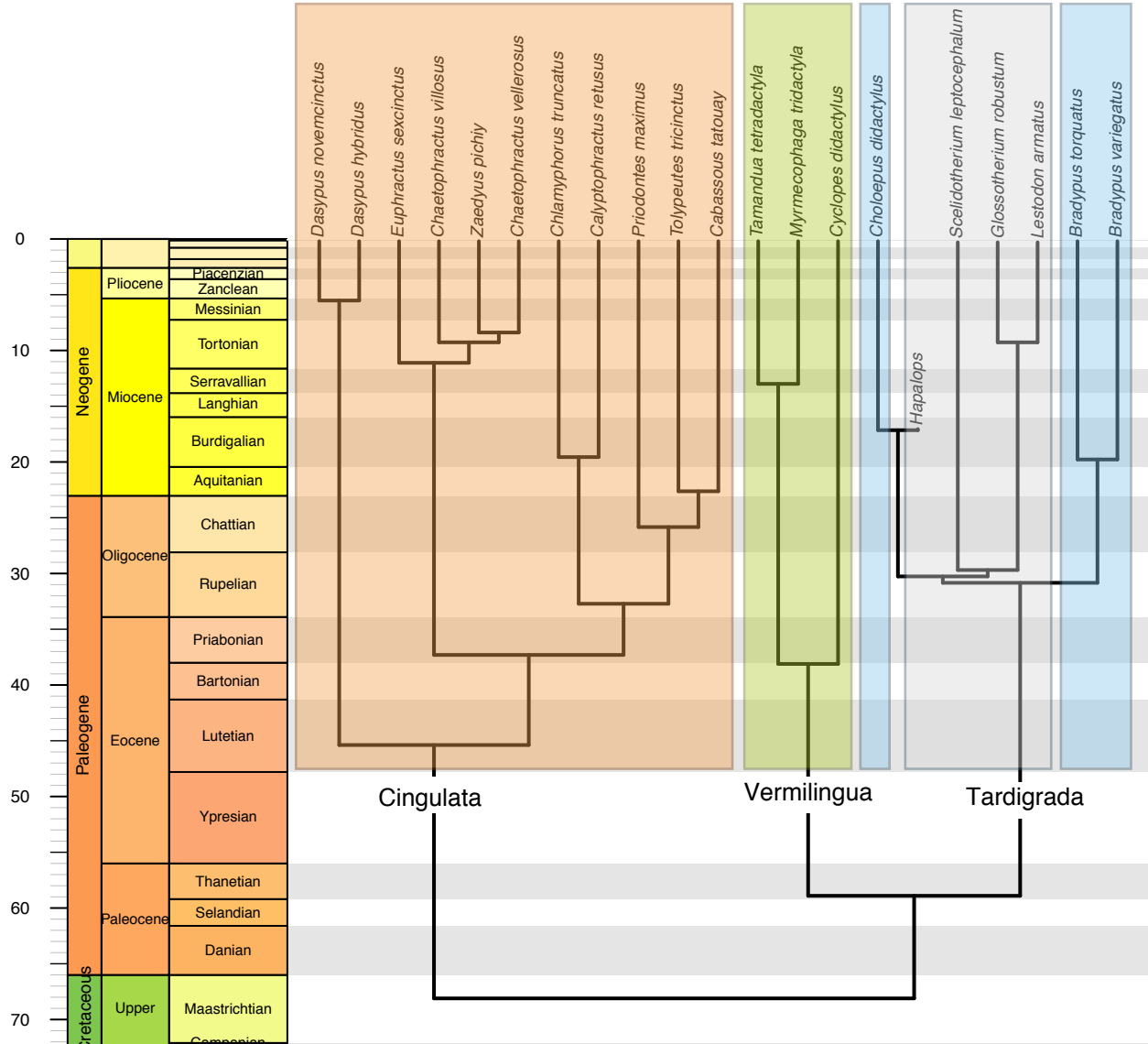
Dasypus novemcinctus
Dasypus hybridus
Euphractus sexcinctus
Chaetophractus villosus
Zaedyus pichiy
Chaetophractus vellerosus
Chlamyphorus truncatus
Calyptophractus retusus
Priodontes maximus
Tolypeutes tricinctus
Cabassous tatouay
Tamandua tetradactyla
Myrmecophaga tridactyla
Cyclopes didactylus
Choloepus didactylus
Hapalops
Scelidotherium leptocephalum
Glossotherium robustum
Lestodon armatus
Bradypus torquatus
Bradypus variegatus
Cingulata
Vermilingua
Tardigrada
0
10
20
30
40
50
60
70
Neogene
Paleogene
Cretaceous
Pliocene
Miocene
Oligocene
Eocene
Paleocene
Upper
Piacenzian
Zanclean
Messinian
Tortonian
Serravallian
Langhian
Burdigalian
Aquitanian
Chattian
Rupelian
Priabonian
Bartonian
Lutetian
Ypresian
Thanetian
Selandian
Danian
Maastrichtian

A
B
C
D
E
F
G

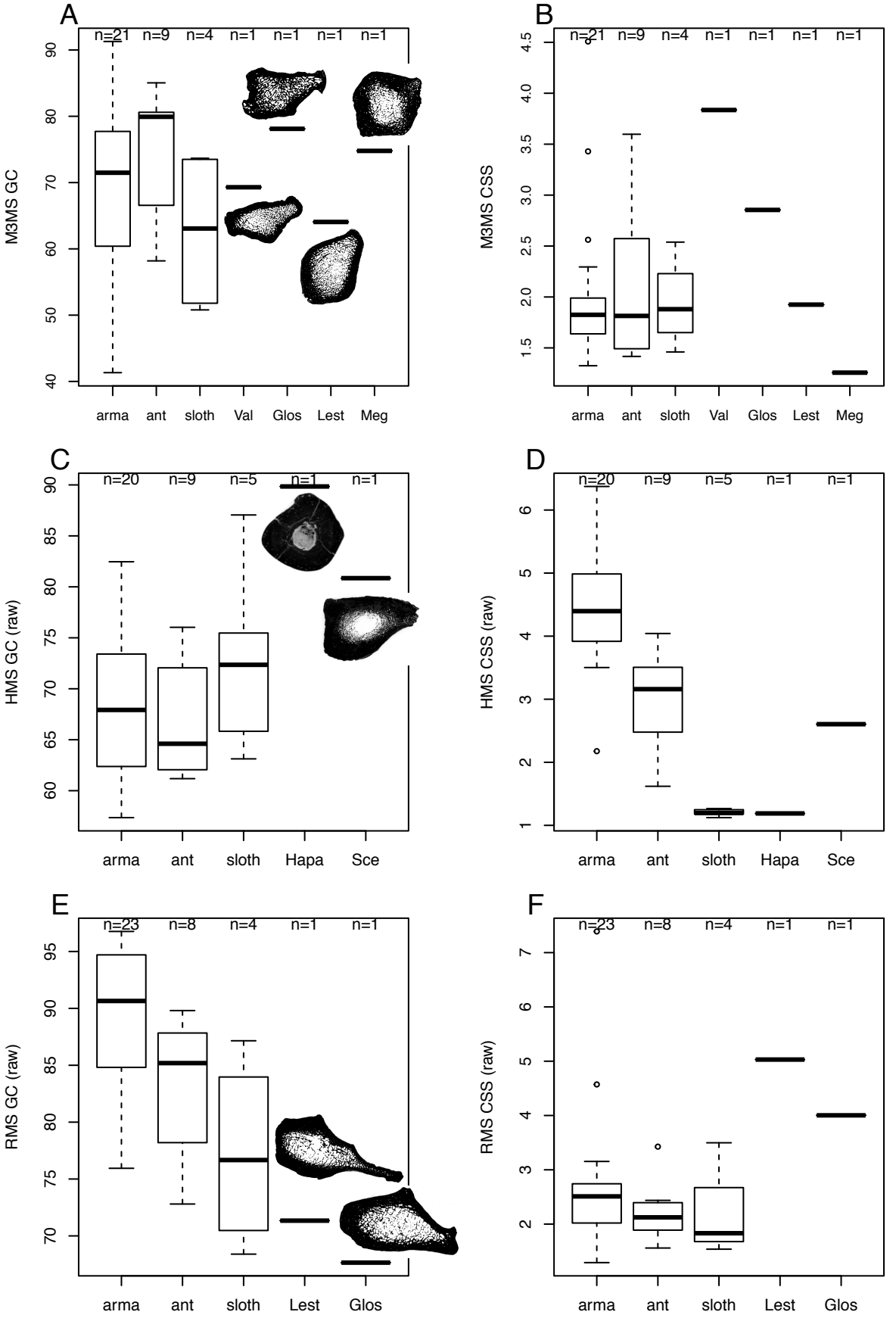
A
n=21 n=9 n=4 n=1 n=1 n=1 n=1
M3MS GC
arma ant sloth Val Glos Lest Meg
B
n=21 n=9 n=4 n=1 n=1 n=1 n=1
M3MS CSS
arma ant sloth Val Glos Lest Meg
C
n=20 n=9 n=5 n=1 n=1
HMS GC (raw)
arma ant sloth Hapa Sce
D
n=20 n=9 n=5 n=1 n=1
HMS CSS (raw)
arma ant sloth Hapa Sce
E
n=23 n=8 n=4 n=1 n=1
RMS GC (raw)
arma ant sloth Lest Glos
F
n=23 n=8 n=4 n=1 n=1
RMS CSS (raw)
arma ant sloth Lest Glos

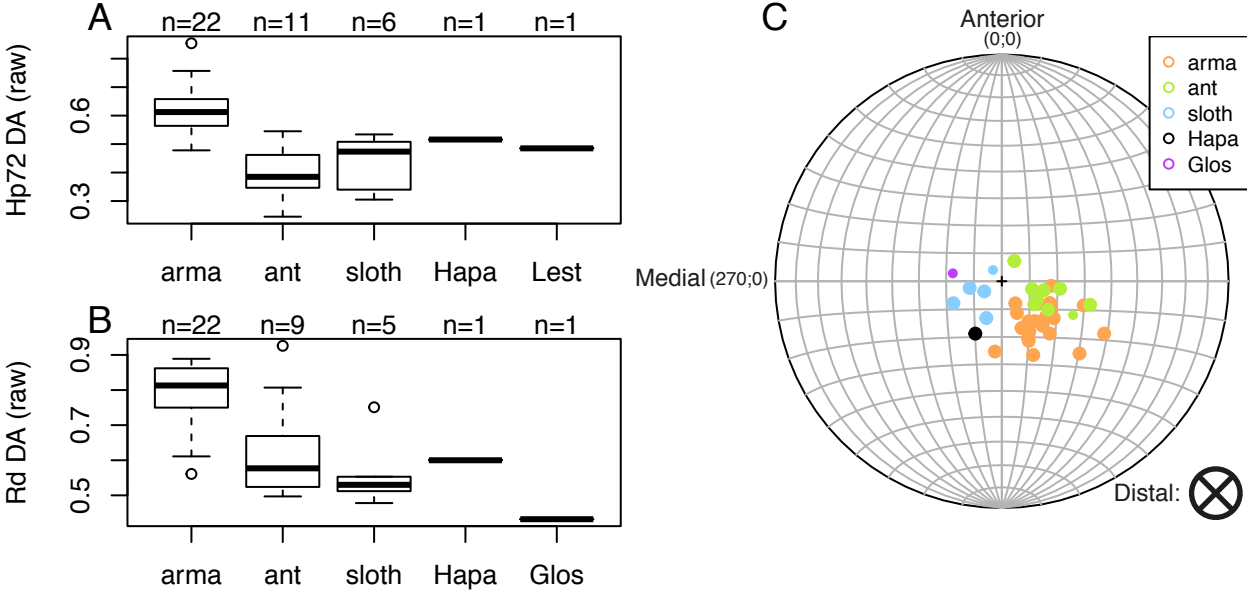
A
n=22
n=11
n=6
n=1
n=1
Hp72 DA (raw)
0.3
0.6
arma
ant
sloth
Hapa
Lest
B
n=22
n=9
n=5
n=1
n=1
Rd DA (raw)
0.5
0.7
0.9
arma
ant
sloth
Hapa
Glos
C
Anterior
(0;0)
Medial (270;0)
Distal:
arma
ant
sloth
Hapa
Glos

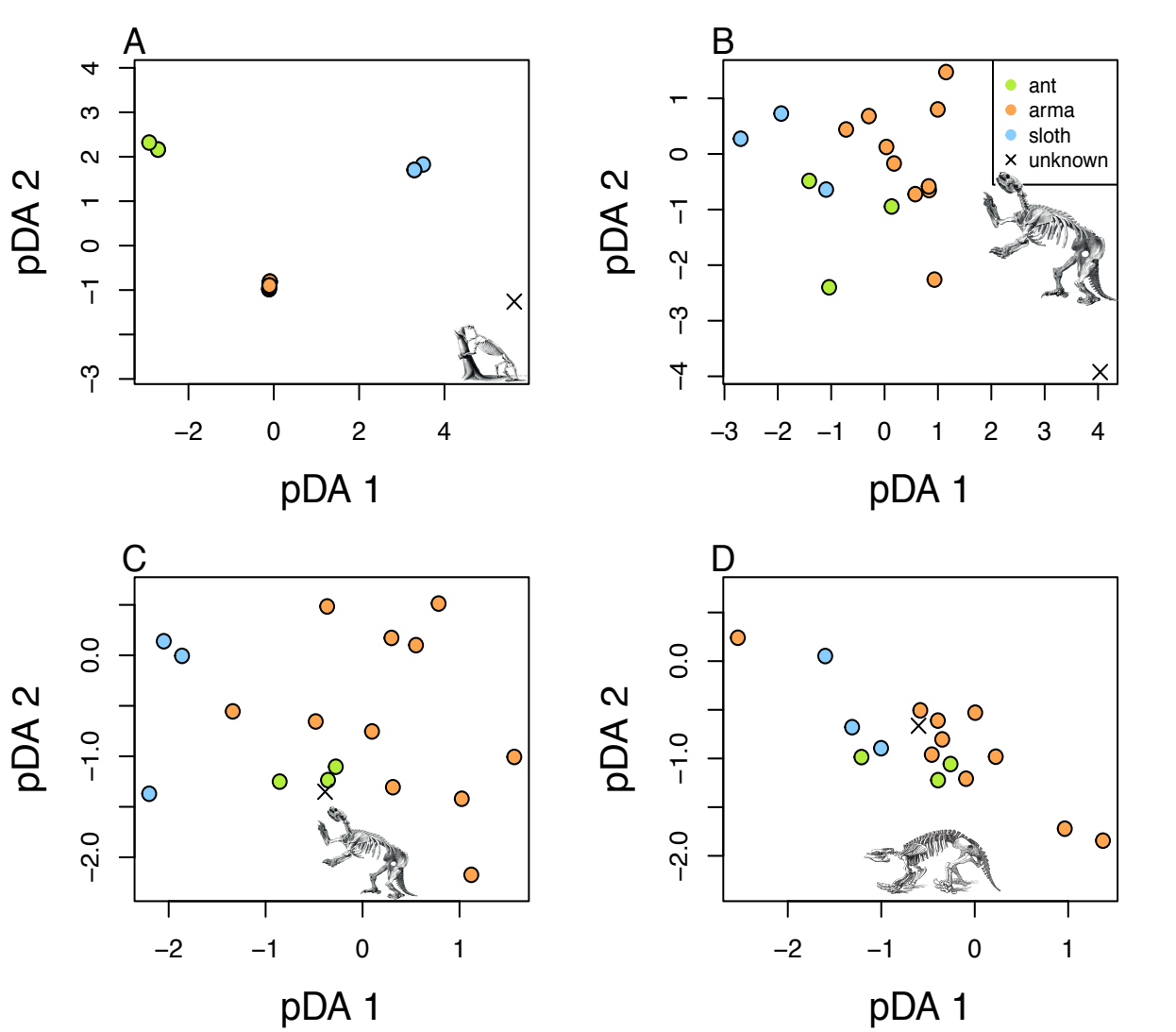
A
B
C
D
pDA 1
pDA 2
ant
arma
sloth
unknown